Accurately Estimating Sherd 3D Surface Geometry with Application to Pot Reconstruction

Andrew Willis †, Xavier Orriols ‡, David B. Cooper †
† Brown University, Providence, RI 02912
‡ Computer Vision Center (UAB), 08193 Bellaterra, Spain

Abstract

This paper deals with the problem of precise automatic estimation of the surface geometry of pot sherds uncovered at archaeological excavation sites using dense 3D laser-scan data. Critical to ceramic fragment analysis is the ability to geometrically classify excavated sherds, and, if possible, reconstruct the original pots using the sherd fragments. To do this, archaelogists must estimate the pot geometry in terms of an axis and associated profile curve from the discovered fragments. In this paper, we discuss an automatic method for accurately estimating an axis/profile curve pair for each archeological sherd (even when they are small) based on axially symmetric implicit polynomial surface models. Our method estimates the axis/profile curve for a sherd by finding the axially symmetric algebraic surface which best fits the measured set of dense 3D points and associated normals. We note that this method will work on 3D point data alone and does not require any local surface computations such as differentiation. Axis/profile curve estimates are accompanied by a detailed statistical error analysis. Estimation and error analysis are illustrated with application to a number of sherds. These fragments, excavated from Petra, Jordan, are chosen as exemplars of the families of geometrically diverse sherds commonly found on an archeological excavation site. We then briefly discuss how the estimation results may be integrated into a larger pot reconstruction program.

1 Archaeological Context

In antiquity, pots and vases were mass-produced by civilizations for use in a variety of contexts. Hence, pieces of pots and vases, hereafter referred to as *sherds,* are prevalent artifacts uncovered in many archaeological excavation sites. By studying these fragments, archaeologists obtain great amounts of information about ancient civilizations. *This paper provides a highly accurate solution to the difficult problem of extracting a geometric model of the unknown pot structure in the region associated with 3D measurements obtained from a sherd. The model extracted may be used in a variety of applications. Some examples are: shape-based searching of 3D sherd databases; sherd classification; and pot reconstruction.* In §7, we touch on the specific application of our models to pot reconstruction.

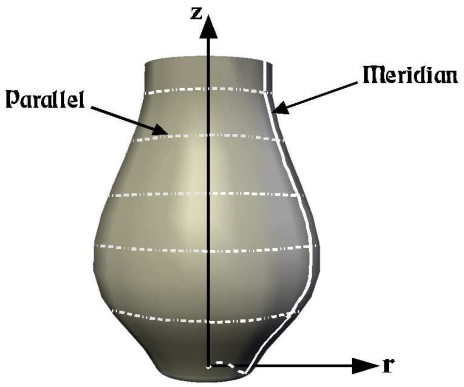

Figure 1: Geometry of a surface of revolution

2 Surfaces of Revolution

The notation and terminology adopted for surfaces in this paper is that used in classic texts such as [10, 7]. A surface of revolution $S \in \Re^3$ is obtained by revolving a planar curve $C \in \Re^2$ about a line $\mathbf{l} \in \Re^3$. α is called the *profile* (or generating) curve and $\mathbf{l}$ the *axis* of S. When the Z-axis is taken as the axis of revolution with profile curve $\alpha(z)$, the surface S may be represented parametrically as

$$S(\theta,\ z) = (\alpha(z)\cos\theta,\ \alpha(z)\sin\theta,\ z) \qquad (1)$$

With this parametrization, the curves $z = constant$ are *parallels* of S and the curves $\theta = constant$ are *meridians* of S. The profile curve characterizes how the radius and height of the surface change for a fixed meridian, see Fig (1). In the literature, [14], an axially symmetric surface is a special case of a Simple Homogeneous Generalized Cylinder, SHGC, one which has circular cross section. In (1), the radius function, $r = \alpha(z)$, is a single-valued function of z. In the case of archaeological sherds, there often occur multiple radius values for a specific height z. Examples include sherds which come from pot bases and rims, see Fig. 3 for

appeared in ACVA (a CVPR Workshop) and from the Proceedings of CVPR (Conference on Computer Vision and Pattern Recognition), June 2003

a typical example of a pot base profile. For this reason, we have generalized our profile curve model to include these situations by using a planar implicit polynomial, i.e. an algebraic planar curve : $\alpha(r, z) = 0$. The problem of interest is: given an unorganized set of 3D measured points of a small patch of a larger axially symmetric surface, estimate a surface geometry model for the patch. We see that this geometry is completely specified by an axis in 3D and a 2D profile curve with respect to that axis. Consequently, estimation of axially symmetric surface models is estimation of axis/profile curve pairs $\{\mathbf{l},\ \alpha(r, z)\}$. Our algorithm seeks the axis/profile curve pair which best fits the measured sherd data.

3 Previous Work

In recent years there has been an increase in research pertaining to the automatic estimation of shape models from 3D surface data. However, in the estimation of axially symmetric shapes, the methods proposed have not been shown to be effective for small surface patches. But these cases are important in practice and challenging in concept. Some initial work on the subject was proposed in [9] where the authors apply concepts from algebraic geometry to develop a linear algorithm for estimating the axis of symmetry. This method has the benefit of providing a quick and reasonable estimate. Yet, in the interest of preserving linear computational complexity, the authors do not enforce the Plücker relation which guarantees that the solution is a valid Euclidean line. Additionally, by estimating the axis as a line intersected by locally estimated surface normals, the method cannot make use of the fact that the measured data lies on a continuous axially symmetric surface patch. Hence, the estimation accuracy is not sufficient for our applications. In [8], a method of axis estimation is presented based on the fact that for a surface of revolution, maximal spheres tangent to the surface will have centers on the axis of symmetry. This method differs from ours since the authors are estimating osculating spheres for each data point/normal pair to obtain an estimate of the axis of symmetry. The centers of these spheres depend upon the principal curvature of the surface parallel which passes through each of the point/normal pairs. The authors add robustness to their estimator by detecting outliers in a weighted iterative least-squares framework. Having computed their axis estimate, the authors then use this estimate to compute the profile curve using a cubic spline model fit to the sherd data. In our case, axially symmetric surfaces are fit to *all* surface data/normal pairs simultaneously using a weighted iterative least-squares fitting method. In doing so, our model incorporates information from *both* the meridians *and* the parallels of the surface of revolution and does not require use of any local operators such as differentiation which amplifies the measurement noise. In §4, we illustrate this distinction between the two methods which lead to different axis/profile estimates. Sherd classification based on qualitative (*e.g.*, global shape) of profiles with human-driven preprocessing is being developed at the Technical University of Vienna [13, 6].

4 Axis / Profile Curve Model

The pose of a rotationally symmetric object is defined up to a sign by it's axis of symmetry. We have parametrized the axis of symmetry using a standard parametric equation of a 3D line:

$$\begin{aligned} x &= m_x z + b_x \\ y &= m_y z + b_y \end{aligned} \tag{2}$$

These equations contain 4 unknown parameters which describe the 3D axis of symmetry, $\mathbf{l} = \{m_x, m_y, b_x, b_y\}$. Two of these parameters, m_x and m_y, describe the slope of the line when it is projected into the XZ-plane and the YZ-plane respectively. The remaining two parameters, b_x and b_y, specify the x and y coordinates where the axis line intercepts the XY-plane at Z=0.

The profile curve is represented using an implicit polynomial curve model, $\alpha(r, z) = 0$. Implicit polynomial curves provide a compact and low computational-cost method of representing shape [12, 2]. In addition, closed-form linear least-squares fitting methods have been developed that provide stable and robust curve and surface fits in the presence of noise [11]. The general form of a 2D implicit polynomial curve of degree d has $[(d + 1)(d + 2)/2]$ unknown coefficients and takes the following form:

$$\alpha_d(r, z) = \sum_{0 \le j+k \le d;\ j,k \ge 0} a_{jk} r^j z^k = 0\,. \tag{3}$$

Here, d is a parameter which is related to the geometric complexity of the pottery sherd to be estimated. Typically one assigns the smallest value to d which is large enough to represent all objects of interest. In this way, objects which may have little geometric complexity are described as degenerate cases of the more complex model. For the artifacts in this paper, all experiments are performed with $d = 6$.

We apply the Gradient-1 fitting algorithm developed in [11] to estimate implicit polynomial models1. The Gradient-1 fitting algorithm appends a penalty term to the usual least-squares objective function (algebraic distance in this case) which makes use of the gradient of the polynomial in order to get a more stable estimate of the curve. This fitting method makes use of all the available information: the hypothesized axis, the measured spatial data and the observed normals. This information is used to compute the global surface model which best fits the data and is symmetric about the hypothesized axis.

appeared in ACVA (a CVPR Workshop) and from the Proceedings of CVPR (Conference on Computer Vision and Pattern Recognition), June 2003

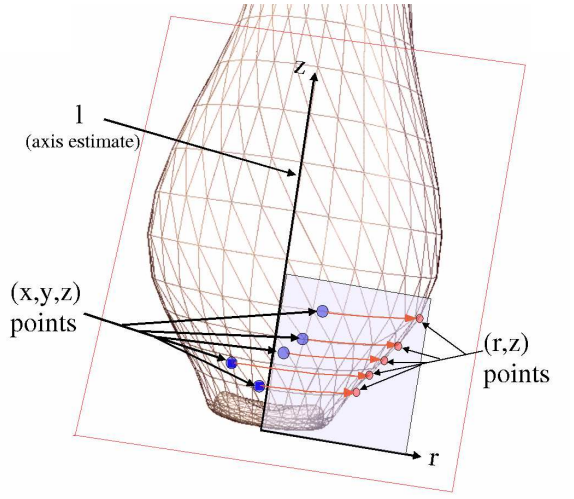

Figure 2: Several (x, y, z) points (in blue) are projected into the (r, z) plane (in red) defined by the estimated axis $\mathbf{l}$ and a vector orthogonal to the axis passing through the data centroid. The highlighted portion is further discussed in Figure (3).

Given an axis of symmetry $\mathbf{l}$, the radius and height position/direction of each 3D sherd point/normal must be computed with respect to the axis $\mathbf{l}$. We denote the i^{th} 3D data point and normal, of the sherd, as $\mathbf{p}_i$ and $\mathbf{n}_i$ respectively. The 2D radius and height for the i^{th} sherd point are referred to as (r_i, z_i) and the corresponding 2D normal is $\mathbf{n}_i^p$. Here, the p superscript denotes projection since the points (r_i, z_i) and $\mathbf{n}_i^p$ can be viewed as an orthogonal projection of the 3D data points into the (r, z) plane of a cylindrical coordinate system whose z-axis is defined by $\mathbf{l}$, and the projection of $\mathbf{n}_i$ into this plane, see Fig. (2). This projection into rz-space preserves the distance relationship between the axis and each point $\mathbf{p}_i$ in xyz-space, but discards the component of the surface normal in the θ direction. Hence, for any 3D normal, $\mathbf{n}_i$, the corresponding projected normal, $\mathbf{n}_i^p$, may not be of unit length, *i.e.*, $\|\mathbf{n}_i^p\| \leq 1$. These parameters define the objective function (4) below, which is a modified version of the energy function in [11], for estimating the profile curve coefficients:

$$e_{grad1} = \sum_{i=1}^{I} (\alpha^2(r_i,\, z_i) + \mu \;\; \|\mathbf{n}_i^p - \nabla\alpha(r_i,\, z_i)\|^2)\,, \quad (4)$$

where $\nabla\alpha(r_i,\, z_i) = \left[\begin{array}{cc} \frac{\partial\alpha}{\partial r} & \frac{\partial\alpha}{\partial z} \end{array}\right]^t$ denotes the gradient. Note that, $\alpha^2(r_i, z_i)$ is the surface point fitting error in (4) and the latter term fits the polynomial normals to the measured surface normals. The value chosen for μ will depend upon the noise present in the measured surface normals. For our experiments, we set $\mu = 0.01$ which corresponds to weighting errors due to the data normals less than errors due to data points. We emphasize again that (4) is an error function for 2D curve fitting that gives exactly the same results as does the error function in [11] for 3D surface fitting.

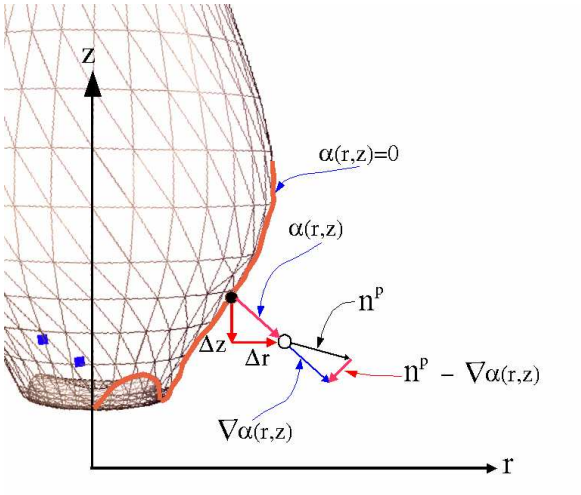

Figure 3: Decomposition of fit error: Here the closest root of a profile curve model, $\alpha(r, z) = 0$, is shown as a solid circle in relation to the single sherd data point, shown as an outlined circle, and normal $\mathbf{n}^p$ in the (r, z) plane. The fitting error between the model and the sherd data is decomposed into two separate terms. $\alpha(r, z)$ provides an approximate measure of the spatial difference between the axially symmetric surface and the measured sherd surface point. $\|\mathbf{n}^p - \nabla\alpha(r, z)\|$ provides a measure of the difference between the axially symmetric surface normal and the measured sherd surface normal.

The scalar residual, e_{grad1}, is a measure of asymmetry resulting from the hypothesized axis. For a specific axis/profile curve model and a data point/normal, the error between the point/normal and the closest point/normal on the profile curve model in radial or r direction is interpreted as asymmetry for a *parallel* of the surface of revolution and error in the height or z direction is interpreted as asymmetry for a *meridian* of the surface. Fig. (3) illustrates these error terms graphically, spatial asymmetry in the directions of the parallel and meridian are indicated with $(\Delta r, \Delta z)$ respectively. The axially symmetric surface fit has a similar error term for differences in measured surface normals and the normals of the estimated surface indicated by $\|\mathbf{n}^p - \nabla\alpha(r, z)\|$. Note that the estimates produced by this method incorporates all of the information available in the data which includes observed variation in *both* of the principal directions of the surface of revolution. We do so without computing any local information from the observed data which makes our estimation procedure robust to noisy

appeared in ACVA (a CVPR Workshop) and from the Proceedings of CVPR (Conference on Computer Vision and Pattern Recognition), June 2003

sherd data.

5 Axis / Profile Estimation

Our method utilitizes a two-step iterative algorithm to estimate the axis and associated profile curve which best describes the observed 3D data.

1. Based on the value of the objective function after the preceding iteration, choose a new value for the axis parameters, $\mathbf{l}$.

2. Based on the new $\mathbf{l}$, compute e_{grad1}, the value of the objective function by solving the weighted linear least-squares problem (4). This is an explicit solution which is a linear function of the data.

Since the surface model depends upon the axis, the resulting objective function is highly non-linear. Consequently, convergence to a local minimum may occur if minimization is started far from the true parameter value.

The estimation algorithm needs only a hypothesized axis of symmetry in order to begin.[1]

6 Experimental Results

A series of experiments were run upon the sherds obtained from an excavation of the Great Temple located in Petra, Jordan [5]. The sherds were scanned by a ShapeGrabber 3D laser scanner which provides surface point and normal measurements for the sherd outer surface [1]. We present results on five sherds which are examples of the families of geometrically diverse sherds commonly found on an archeological excavation site. For each of these sherds we have performed detailed error analysis which we then discuss.

Error analysis proceeds by applying the bootstrap method with a sample size of 500. Each bootstrap sample uses the same number of points and normals as the original sherd data set and is generated by a random resampling of the sherd point/normal data where a single data point may be selected more than once [3]. For each of the 500 bootstrap samples, an axis/profile curve estimate is generated. We denote the i^{th} bootstrap estimate as $\{\mathbf{l}_i, \alpha_i(r,z)\}$. We assume that the resulting 500 axis/profile curve estimates represent independent samples taken from a multivariate normal distribution with mean μ and covariance Σ. Hence, we may compute an estimate of the axis/profile curve distribution by computing the estimated mean $\widehat{\mu} = \{\widehat{\mathbf{l}}, \widehat{\alpha(r,z)}\}$ and covariance $\widehat{\Sigma}$ which provides us with an approximation $\sim \mathcal{N}(\widehat{\mu}, \widehat{\Sigma})$ of the true distribution of the axis/profile curve parameters. Note, the error function we minimize could result in slightly biased estimates. Hence, the most important use of the bootstrap results is estimating the posterior probability density function for the axis/profile curve given the 3D measurement data set. This information seems to be very important in deciding on the confidence the system can have in hypothesized configurations of sherds which is crucial in pot assembly from sherds. Understanding the bias in the estimates is obtained by looking at the 3D-measurement data scatter about the maximum likelihood estimate of the axis/profile-curve specified 3D surface.

For the purpose of comparing results between sherds of different shapes and sizes we defined a global coordinate system in which to analyze the axis/profile curve parameters for all sherds. This coordinate system transforms the sherd data such that the mean estimated axis, $\widehat{\mathbf{l}}$, is the world coordinate z-axis and the sherd data centroid lies on the x-axis.

Three sets of information are presented with an image of each measured sherd : 1) covariance matrix for axis parameters (m_x, b_x, m_y, b_y); 2) three profile curves, each associated with an axis estimate representing a 95% confidence interval for the axis estimates; 3) A plot of the standard deviation of the laser scan 3D data points with respect to the mean profile curve estimate, as a function of height, z, along the mean estimate of the pot axis.

In order to compute the 95% confidence interval, the slope parameters of the axis, (m_x, m_y), from (2) were normalized by the height extent of the sherd. The new axis parametrization is given by (5).

$$\begin{aligned} x &= \frac{m_x}{z_0} z + b_x \\ y &= \frac{m_y}{z_0} z + b_y \end{aligned} \tag{5}$$

Here z_0 denotes the height range spanned by the profile of a sherd with respect to it's mean estimated axis. This normalization changes the axis slope parameters (m_x, m_y) into parameters which represent the change in axis direction as a percentage of the sherd height. This provides a meaningful measure which has units, $\frac{\%sherd\ height}{mm.}$, for those components of the eigenvector which characterize the directions of the axis. For the parameter m_x, the normalized parameter $\frac{m_x}{z_0}$ represents the change in axis direction in the XZ-plane as the ratio of a percentage of the sherd height per incremental step, Δx, in the direction of the x-axis: $\frac{\Delta z(\%)}{\Delta x(mm.)}$.

Having normalized our axis directional parameters, we proceed by taking the eigenvector associated with the maximum eigenvalue of the axis parameter covariance matrix and choose parameters which are at the two ends of the

[1] Typically, our initial axis estimate is obtained using the linear algorithm described in [9]. However, an additional validation step is applied to detect degenerate surfaces of revolution by determining if the sherd data is well approximated by a sphere, hyper ellipsoid, or saddle surface. If the sherd data is determined to be spherical in nature, then no axis is estimated. If the sherd data lies on a saddle surface or an ellipsoid, then there are two or three valid axis estimates respectively. In these cases additional information is necessary to determine the true axis of symmetry for the sherd.

appeared in ACVA (a CVPR Workshop) and from the Proceedings of CVPR (Conference on Computer Vision and Pattern Recognition), June 2003

95% confidence interval in the direction of the eigenvector (shown in blue and green), and the third axis parameter vector is the mean of the distribution (in red). The three profile curves shown are those associated with these three axes respectively.

An additional figure (9) is provided to provide perspective on the axis estimates which are obtained via our method. For Figs. (4-8), plotted profile curves are zoomed to accentuate the source of the small observed errors in the estimates. Since variations typically range between 0.3-0.001 mm., without zooming in closely to examine small fluctuations, it is difficult to discern any variation in the three 95% confidence interval profile curves for a sherd.

In Fig. (9), we show a non-scaled version of the original 3D data points which have been rotated into the (r, z) plane. The y-axis is height along the estimated axis, and the x-axis is distance from the estimated sherd axis for each 3D data point. The best axis estimate will be that for which the scatter is smallest locally in the direction perpendicular to the true surface. The data scatter for sherds 967 and 1313 is shown in Fig. (9). What is amazing is the small data scatter-especially in Fig (9a) where the sherd is almost horizontal with respect to it's estimated axis. Qualitative confidence in the axis direction estimation is obtained by observing rings on the inside of the sherd resulting from pot construction on a spinning wheel.

0.0111	-0.0661	0.0002	-0.0005
-0.0661	0.4179	-0.0004	-0.0022
0.0002	-0.0004	0.0002	-0.0015
-0.0005	-0.0022	-0.0015	0.0100

(a) Sherd image (b) Axis parameters covariance matrix (mm.)

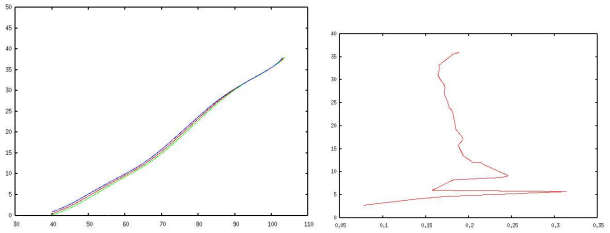

(c) 95% confidence interval (mm.) (d) standard deviation (mm.)

Figure 4: Experimental Results for sherd 654

Fig. (4) : the sherd profile curve has a simple shape which is commonly associated with body sherds found at a typical archaeological excavation. Since curvatures are small in direction of both sherd meridians and sherd parallels, axis estimates here are difficult. Our accuracy in estimating the axis of this piece demonstrates robustness to data noise.

0.0290	-0.1748	-0.0034	0.0264
-0.1748	1.6484	0.0389	-0.3441
-0.0034	0.0389	0.0013	-0.0109
0.0264	-0.3441	-0.0109	0.0979

(a) Sherd image (b) Axis parameters covariance matrix (mm.)

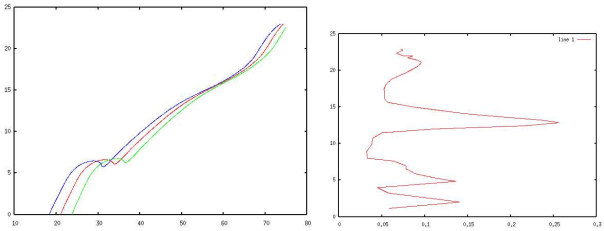

(c) 95% confidence interval (mm.) (d) standard deviation (mm.)

Figure 5: Experimental Results for sherd 967

0.0979	-0.5373	-0.0255	0.1404
-0.5373	2.9906	0.1406	-0.7820
-0.0255	0.1406	0.0069	-0.0380
0.1404	-0.7820	-0.0380	0.2111

(a) Sherd image (b) Axis parameters covariance matrix (mm.)

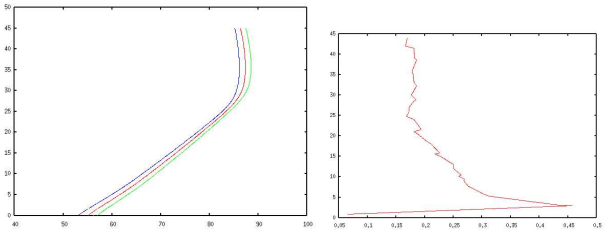

(c) 95% confidence interval (mm.) (d) standard deviation (mm.)

Figure 6: Experimental Results for sherd 997

Fig (5) : the sherd has parallels with small curvatures, yet the meridians of this sherd have significant curvature information. Since this piece is very small, has a multiple-valued profile curve, and has normals which are close to parallel to the axis of symmetry, estimation here is especially difficult for methods based on surface normal lines. Since our method incorporates normal information differently, these

appeared in ACVA (a CVPR Workshop) and from the Proceedings of CVPR (Conference on Computer Vision and Pattern Recognition), June 2003

0.0042	-0.0026	0.0001	0.0004
-0.0026	0.0031	0.0003	-0.0004
0.0001	0.0003	0.0002	-0.0001
0.0004	-0.0004	-0.0001	0.0002

(a) Sherd image (b) Axis parameters covariance matrix (mm.)

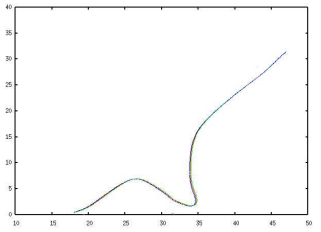

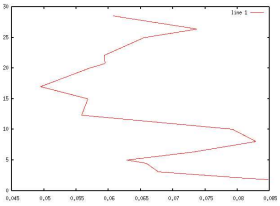

(c) 95% confidence interval (mm.) (d) standard deviation (mm.)

Figure 7: Experimental Results for sherd 1135

0.2317	-0.0771	0.0193	-0.0076
-0.0771	0.0715	-0.0078	0.0058
0.0193	-0.0078	0.0088	-0.0027
-0.0076	0.0058	-0.0027	0.0022

(a) Sherd image (b) Axis parameters covariance matrix (mm.)

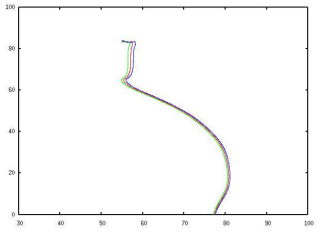

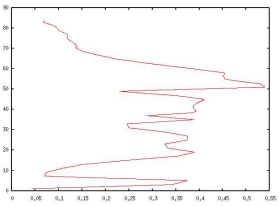

(c) 95% confidence interval (mm.) (d) standard deviation (mm.)

Figure 8: Experimental Results for sherd 1313

apparent obstacles do not cause problems for our axis estimation method. Uncertainty in the axis location is represented by parallel profile curves in (c) and again in (b) by examining elements (2,2) and (4,4) of the axis parameter covariance matrix.

Fig (6) : the sherd here has small curvatures along sherd parallels and a small region of high curvature along sherd meridians. As in Fig. (5), we see that when there is little

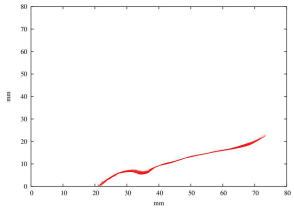

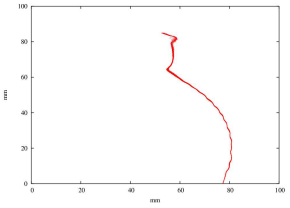

(a) p967 data projection (mm.) (b) p1313 data projection (mm.)

Figure 9: Sherd data projected into (r, z) plane using the mean axis estimate.

data (i.e. a small sherd) combined with small curvatures in the direction of the sherd parallels, it is difficult to accurately estimate the axis location. This is evident in the parallel translations of the profile curves in (c) as well as in (b) by examining the covariance matrix. This leads to an important inference: *Sherds which have little data with respect to their subtended angle about the axis of revolution and small curvatures in the direction of the surface parallels have more variation in their axis location parameters* (b_x, b_y).

Fig (7) : the sherd here has highly curved parallels and meridians. Yet the sherd ridges are chipped and worn (see part (a)) which generates a large amount of asymmetric data measurements. Our axis/profile curve estimates here are very accurate which reflects good robustness to asymmetry in regions of high curvature and to local surface noise.

Fig. (8) : the sherd has high frequency information in the sherd meridians in the form of a ripple and two high curvature points at the apparent pot rim (see (a)). Since the large majority of the sherd is well approximated by an ellipsoid (see (c)), determining a unque axis direction here is difficult and relies almost exclusively on data measurements obtained at the rim. Our method uses the global sherd information to provide an accurate and stable axis/profile curve estimate.

7 Pot Reconstruction

Denote (all) the available geometric data by $\Theta_{i,j}$, which consits of the break-curve data $\Phi_{i,j}$ and the surface data $\Omega_{i,j}$, this for sherds i and j. Then alignment and pot model estimation for sherd i and j data sets jointly is done by the minimization over all geometric parameters:

$$\begin{aligned} &\min\left[-\log P\left\{\Theta_{i,j} \mid \beta_{ij}\mathbf{l}_{ij}, \mathbf{T}_i, \mathbf{T}_j, \alpha_{ij}\right\}\right] = \\ &\min\left[-\log P\left\{\Phi_{i,j} \mid \mathbf{T}_i, \mathbf{T}_j\right\} - \log P\left\{\Omega_{i,j} \mid \mathbf{T}_i, \mathbf{T}_j, \mathbf{l}_{ij}, \alpha_{ij}\right\}\right] = \\ &e_{\mathbf{T}} + e_{grad1} + \text{constant}\,, \end{aligned} \tag{6}$$

where $e_{\mathbf{T}}$ is an energy function of the sherd boundary data. The geometric parameters here are the joint sherd axis

appeared in ACVA (a CVPR Workshop) and from the Proceedings of CVPR (Conference on Computer Vision and Pattern Recognition), June 2003

$\mathbf{l}_{i,j}$, the joint sherd profile curve $\alpha_{i,j}$, the break curve $\beta_{i,j}$ shared by sherd i and sherd j (i.e. the curve on the pot surface along which sherds i and j broke) and $\mathbf{T}_i$ and $\mathbf{T}_j$ which are the Euclidean transformations to put sherds i and j, respectively, together to estimate a pot model in standard position, i.e., having it's axis as the z-axis of the world coordinate system. Maximization of (6) is MLE (maximum likelihood estimation) of the geometric parameters for the configuration of sherds i and j. (6) is our sherd-configuration performance functional. It extends trivially to large configurations of sherds. MLE pot reconstruction is finding configurations for which (6) is a maximum. The implemented algorithm uses approximations for doing the minimization, is computationally fast, and is reasonably accurate for the few examples tried. Note, the approximate probability functions to be used in (6) are obtained from the bootstrapping described in §6 : (see [4] for how to specify (6) in terms of the original data points).

8 Conclusion

We have presented a highly accurate method for automatically estimating axially symmetric surface models for dense 3D laser scanner data taken of pot sherds. The end result is an axis/profile curve pair for a sherd, and this completely specifies the sherd surface geometry. If desired, the accuracy of an estimate can be even further improved by not using data, in the estimation procedure, that occurs at high-curvature points on the sherd surface. This data can be easily automatically identified by detecting data outliers with respect to the profile curve models that we presently estimate. Our axis/profile curve estimates are close to being maximum likelihood estimates, and should therefore be close to maximum accuracy because MLEs are known to be asymptotically of minimum variance, and the number of data points we use in estimating sherd geometry is of the order of 10,000. We estimated multivariate Gaussian distributions for the sherd axis and for some of the sherd profile curve parameters, and related some aspects of sherd geometries to these distributions. Finally, these distributions are important for pot reconstruction because they tell the reconstruction algorithm how much confidence it can have in various estimated parameters. This material is based upon work supported by the National Science Foundation under Grant No. 0205477.

References

[1] Shapegrabber inc. http://www.shapegrabber.com.

[2] M. Blane et al. The 3L algorithm for fitting implicit polynomial curves and surfaces to data. *IEEE Trans. on Pattern Anal. Machine Intell.*, 22(3):298–313, March 2000.

[3] W. J. Conover. *Practical Nonparametric Statistics*. John Wiley & Sons, Inc., 1999.

[4] D. Cooper, A. Willis, Y. Cao, D. Han, F. Leymarie, X. Orriols, D. Mumford, et al. Assembling virtual pots from 3D measurements of their fragments. In *VAST International Symposium on Virtual Reality Archaeology and Cultural Heritage*, pages pp. 241–253, 2001.

[5] M. S. Joukowsky. *Petra Great Temple - Volume 1: Brown University Excavations 1993-1997*. Petra Exploration Fund, Providence, RI, USA, 1999. 390 pages.

[6] M. Kampel and R. Sablatnig. Automated segmentation of archaeological profiles for classification. In *ICPR*, volume I, pages pp. 57–60, 2002.

[7] E. Kreyszig. *Differential Geometry*, pages 128–129. Dover, 1963.

[8] D. Mumford and Y. Cao. Geometric structure estimation of axially symmetric pots from small fragments. In *Proc. of Int. Conf. on Signal Processing, Pattern Recognition, and Applications*, pages 92–97, 2002.

[9] H. Pottmann, M. Peternell, and B. Ravani. An introduction to line geometry with applications. *Computer-Aided Design*, 31:3–16, 1999.

[10] D. J. Struik. *Lectures on Classical Differential Geometry*. Dover, NY, 1950.

[11] T. Tasdizen, J. P. Tarel, and D. B. Cooper. Improving the stability of algebraic curves for applications. *IEEE Trans. on Image Proc.*, 9(3):405–416, March 2000.

[12] G. Taubin. Estimation of planar curves, surfaces and nonplanar space curves defined by implicit equations with applications to edge and range image segmentation. *IEEE Trans. on Pattern Anal. Machine Intell.*, 13(11):1115–1138, November 1991.

[13] S. Tosovic and R. Sablatnig. 3D modeling of archaeological vessels using shape from silhouette. In *Third International Conference on 3D Digital Imaging and Modeling*, Quebec, Canada, June 2001.

[14] M. Zerroug and R. Nevatia. Part-based 3D descriptions of complex objects from a single image. *IEEE Trans. on Pattern Analysi and Machine Intelligence*, 21(9):835–848, September 1999.